Journal of Nanobiotechnology

RESEARCH Open Access

Novel cocktail therapy based on multifunctional supramolecular hydrogel targeting immune-angiogenesis-nerve network for enhanced diabetic wound healing

Ruiyin Zeng[1†], Yuan Xiong[2†], Ze Lin[1†], Xiangyu Chu[1†], Bin Lv[1], Li Lu[1], Chuanlu Lin[1], Jiewen Liao[1], Lizhi Ouyang[1], Yun Sun[3*], Guandong Dai[4*], Faqi Cao[1*] and Guohui Liu[1*]

Abstract

Diabetes-associated chronic skin wounds present a formidable challenge due to inadequate angiogenesis and nerve regeneration during the healing process. In the present study, we introduce a groundbreaking approach in the form of a novel cocktail therapy utilizing a multifunctional supramolecular hydrogel. Formulated through the photo-crosslinking of gelatinized aromatic residues and β-cyclodextrin (β-CD), this injectable hydrogel fosters weak host-guest interactions, offering a promising solution. The therapeutic efficacy of the hydrogel is realized through its integration with adipose-derived stem cells (ADSCs) and lipid nanoparticles encapsulating ginsenoside RG1 and Stromal cell-derived factor-1 (SDF-1). This strategic combination directs ADSCs to the injury site, guiding them toward neurogenic specialization while establishing an advantageous immunomodulatory environment through macrophage reprogramming. The synergistic effects of the newly differentiated nerve cells and the regenerative cytokines secreted by ADSCs contribute significantly to enhanced angiogenesis, ultimately expediting the diabetic wound healing process. To summarize, this innovative hydrogel-based therapeutic system represents a novel perspective for the management of diabetic wounds by concurrently targeting immune response, angiogenesis, and nerve regeneration—a pivotal advancement in the quest for effective solutions in diabetic wound care.

Keywords Diabetes, Hydrogel, Neural differentiation, ADSCs, Macrophage polarization, Wound healing

†Ruiyin Zeng, Yuan Xiong, Ze Lin and Xiangyu Chu contributed equally to this work.

*Correspondence:
Yun Sun
627224540@qq.com
Guandong Dai
kerdong1976@hotmail.com
Faqi Cao
13971293030@qq.com
Guohui Liu
liuguohui@hust.edu.cn

[1]Department of Orthopedics, Union Hospital, Tongji Medical College, Huazhong University of Science and Technology, Wuhan 430022, China
[2]Department of Orthopedics, Tongji Hospital, Tongji Medical College, Huazhong University of Science and Technology, Wuhan 430030, China
[3]Department of Neurosurgery, Union Hospital, Tongji Medical College, Huazhong University of Science and Technology, Wuhan 430022, China
[4]Department of Orthopaedics, Pingshan District People's Hospital of Shenzhen, Pingshan General Hospital of Southern Medical University, Shenzhen 518118, Guangdong, China

Introduction

Patients with diabetes often suffer from chronic, non-healing skin and soft tissue wounds, which are prone to infection and are difficult to treat clinically, significantly reducing the patient's quality of life [1]. The nervous system and the vascular system have a close and intricate relationship, playing a crucial regulatory role in the process of wound healing. Surrounding neurons in the skin regulate vascular tone, hemodynamics, and vascular growth and function through the release of growth factors and neuropeptides. Additionally, they can also modulate local immunity and inflammation. Conversely, the vascular system is responsible for providing adequate blood supply, including oxygen, nutrients, and growth factors, for tissue repair and growth. Endothelial cells within the blood vessels can also secrete factors that regulate the growth and migration of nerve cells [2, 3].

Angiogenesis and neovascularization are essential processes in the wound healing process. However, metabolic abnormalities in diabetic patients can lead to microvascular disease and diabetic neuropathy [4]. Therefore, in effective wound repair, a synergistic strategies for vascular regeneration and nerve regeneration is necessary to promote tissue regeneration and wound healing [5, 6].

Adipose-derived stromal cells/mesenchymal stem cells (ADSCs), derived from adipose tissue, have the capacity to self-renew and differentiate into different cell lineages. ADSCs play important roles in wound healing and scar formation by promoting angiogenesis (partially through the secretion of extracellular vesicles) and regulating endothelial cells [7, 8]. Furthermore, ADSCs can differentiate into non-mesenchymal cell lineages, such as endothelial cells, myogenic cells, and neuronal lineages [7]. For example, ADSCs differentiate into nerve cells that promote spinal cord repair which underscore their versatile potential [9]. However, its application in wound repair remains an area of ongoing exploration and investigation.

Ginseng, a perennial herbaceous plant belonging to the Araliaceae family, is a commonly used medicinal herb in China. The main active component of ginseng is ginsenoside, which is primarily used in clinical treatments related to the nervous system, cardiovascular system, and anti-tumor effects [10]. Several studies have indicated that ginsenoside Rg1 has the ability to enhance the in vitro proliferation and neurogenic differentiation of ADSCs [11–13]. Additionally, ginsenoside Rg1 can improve the symptoms of various diseases by regulating the polarization balance of M1/M2 macrophages [14, 15]. CXCL12, also known as stromal cell-derived factor-1 (SDF-1), is a small protein belonging to the CXC chemokine subfamily. Studies have indicated that SDF-1/CXCL12 can act as a homing factor for stem cells, enhancing the repair mechanism by recruiting progenitor cells to the site of blood vessels and tissue damage [16, 17]. The chemotactic impact has been shown to influence different categories of stem cells, such as ADSCs, BMSCs, and DPSCs [18–20].

Hence, our objective is to establish a transportation system for the continuous release of RG1 and SDF-1, thereby facilitating the migration of ADSCs toward the injured area and promoting their transformation into nerve cells, ultimately enhancing wound healing through the neurovascular pathway [5]. Nonetheless, the transportation of curative substances is frequently impeded by the swift dispersion and function of protein-digesting enzymes, particularly in persistent inflammatory settings [21]. Hence, one of the primary obstacles in delivering proteins locally is to ensure controlled release at optimal levels, while reducing degradation and diffusion to a minimum. Because of their biocompatibility and capacity to shield and transport protein or small molecule cargos with various physical characteristics, liposomes are extremely attractive for this method [22]. In order to prolong the localized release, drug-filled liposomes can be mixed with a hydrogel to physically capture the enclosed substance and maintain release at levels that promote physiological function.

Therefore, we have developed a hydrogel composite therapeutic delivery system that allows controlled release of the pro-healing chemotactic factor SDF-1α and the pro-neuronal differentiation compound ginsenoside Rg1 to induce the migration and differentiation of ADSCs. To protect the drugs from hydrolytic degradation and regulate their release, we loaded ginsenoside Rg1 and SDF-1α into anionic liposomes and embedded the liposomes with ADSCs into a specially designed injectable light-crosslinked hydrogel formed by weak host-guest interactions, creating a nano-composite hydrogel. Our research aims to further elucidate the roles of natural collagen hydrogel and ADSCs in guiding wound healing and provide insights for the development of clinical treatment delivery strategies (Scheme 1).

Results

Construction and characterization of hydrogels

To begin, a predetermined amount of acrylic-functionalized β-cyclodextrin (Ac-β-CD) was synthesized. Then, gelatin and Ac-β-CD were mixed according to predetermined ratios and controlled conditions. Subsequently, a photoinitiator was added to the mixture. Finally, the mixture was exposed to light irradiation at a wavelength of 390 nm to prepare gelatin-based hydrogels. These hydrogels exhibited enhanced mechanical properties. Scanning Electron Microscope (SEM) picture of the hydrogel's internal microstructure (Fig. 1A) reveals a network of interconnected pores that are advantageous for cell customization and migration. In rheological measurements, the modulus of the gelatin hydrogel increases with the

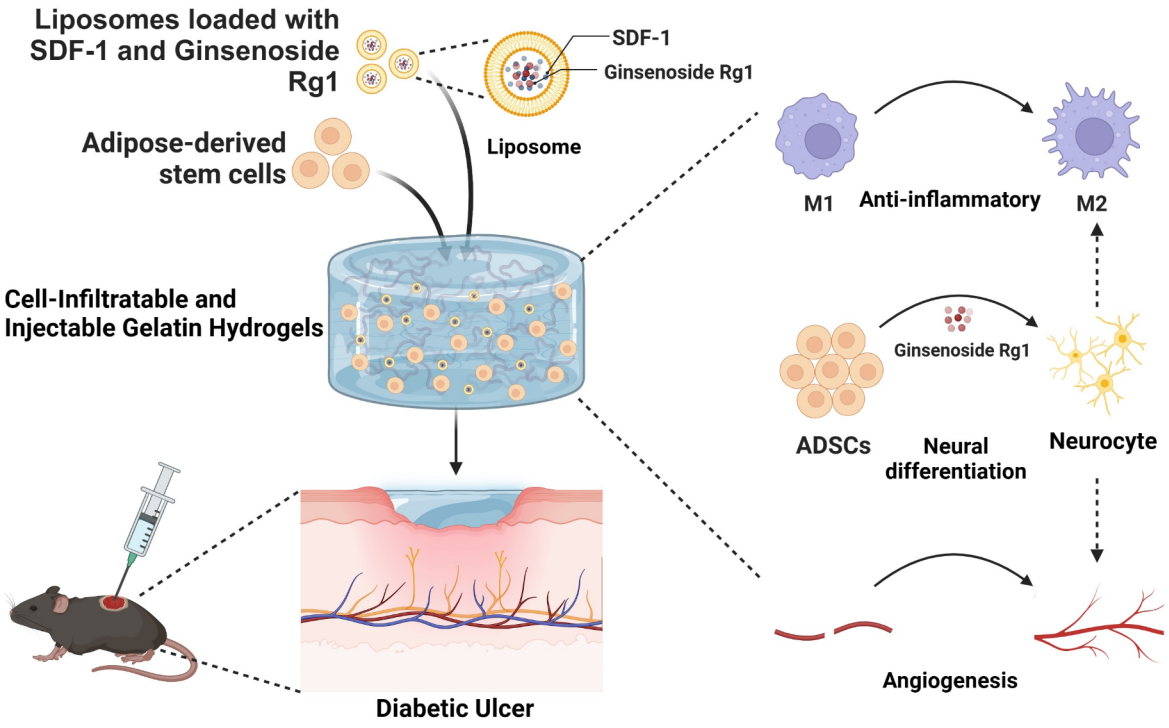

Scheme 1 The preparation of injectable light-crosslinked hydrogels, and their utilization as therapeutic carriers (cells and drugs) for treating diabetes wounds in diabetic mouse models. A schematic illustration demonstrates controlled release of adipose-derived stem cells, CXCL12, and Rg1 from the hydrogel, promoting angiogenesis and neural regeneration at the injury site

change of frequency (Fig. 1B). This observation indicates that the participation of the physical host-guest complexation between the aromatic groups of gelatin and β-CDs makes the hydrogel network unstable. Additional rheological investigations demonstrated a sol-gel transition of the hydrogel when subjected to alternating high and low shear strains (Fig. 1C). Under high shear strain ($G'' > G'$), the hydrogel underwent a transition to a 'sol' state, which was promptly reversed to a 'gel' state when subjected to subsequent low shear strain ($G' > G''$). Additionally, despite undergoing multiple rounds of intense shear loading, the hydrogel's storage modulus (G') eventually reverted back to levels similar to those of unloaded samples that were recently tested. The slight reduction in storage modulus could be due to the partial disturbance of the chemical crosslinking during the application of load. The hydrogel can be injected without causing significant changes to its mechanical performance due to its remarkable ability to undergo shear thinning and self-healing. Furthermore, compressive stress tests demonstrated that the hydrogel could withstand over 70% compressive strain without fracturing (Fig. 1D). Moreover, following the initial loading-unloading cycle, the hydrogel displayed a nearly identical stress-strain curve compared to the subsequent loading cycles, demonstrating exceptional durability against repetitive compressive loading (peak strain 70%) (Fig. 1E). The swelling curve of the hydrogel demonstrated a notable increase in swelling ratio within the initial 6 h, followed by a slow ascent (Figure S1A), whereas the degradation curve exhibited a gradually degrading tendency commencing from 2 days later (Figure S1B). Pre-formed rectangular hydrogels were aspirated into a syringe using a 20G needle and subsequently injected into an 8.5 mm circular well plate, effectively reshaping the hydrogel into a cylindrical form (Fig. 1F). This observation attests to the exceptional moldability and injectability of the hydrogel. After co-culturing the gelatin hydrogel with ADSCs cells for 1 day and 3 days respectively and conducting Calcein/PI staining, the results demonstrated the low toxicity and excellent biocompatibility of the hydrogel (Fig. 1G). Additionally, we cultured the gelatin hydrogel containing ADSCs for 1 day before and after injection to investigate the ability of the hydrogel to maintain the viability of coated cells during injection, and the results showed that the injectable hydrogel had a significant protective effect on ADSCs (Fig. 1G, H).

Synthesis and characterization of composite liposomes

In order to safeguard pharmaceuticals from hydrolytic deterioration and regulate their discharge, we fabricated nanoliposomes that enclose SDF-1α and ginsenoside

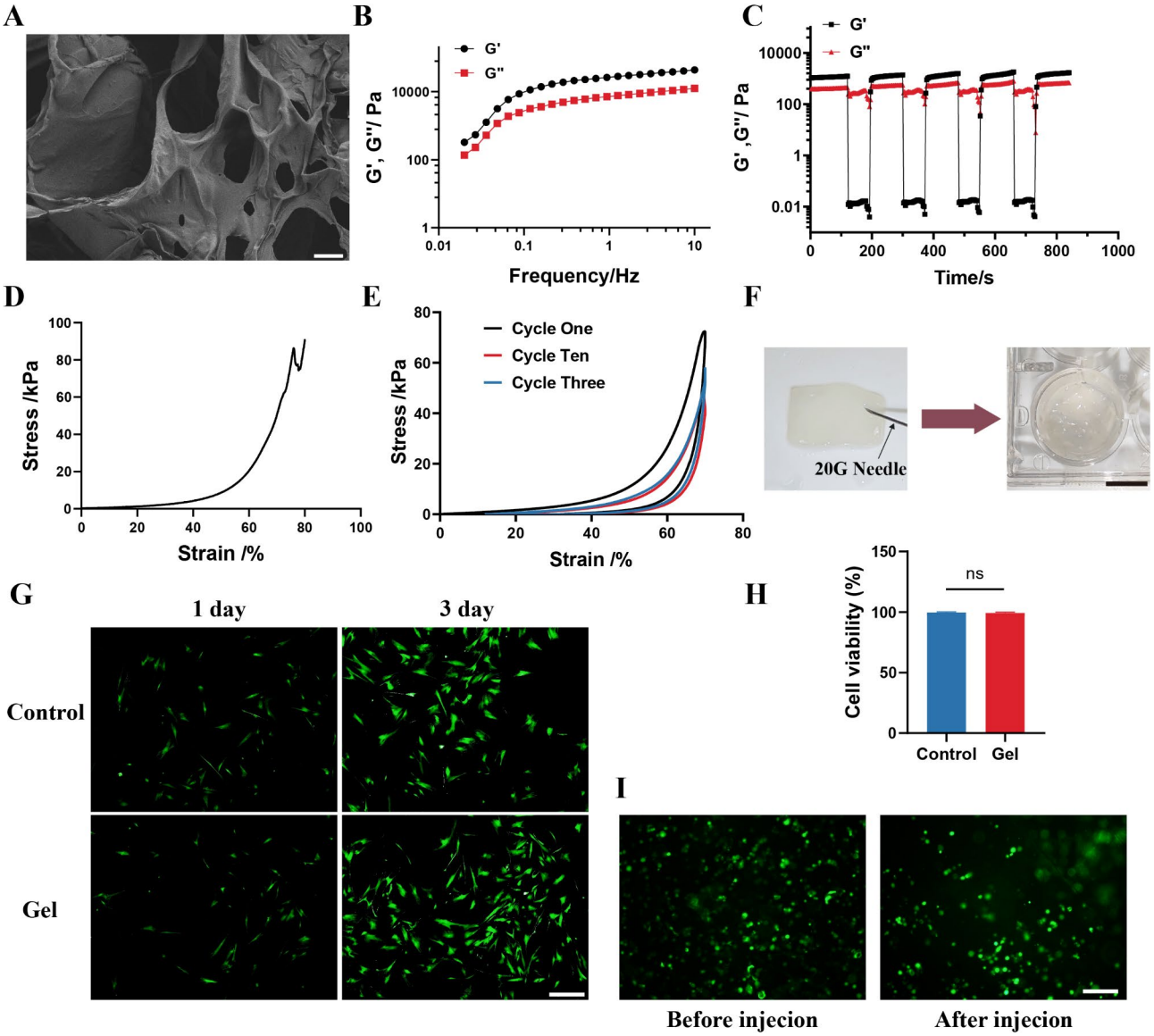

Fig. 1 Hydrogel characterization. (**A**) The SEM images of the hydrogel. (**B**) The hydrogel exhibited a response that varied with frequency during the rheological frequency sweep test, with a strain of 0.1%. (**C**) The study of rheology presents proof of the sol-gel transformation in the supramolecular hydrogels under the influence of alternating high and low shear strain. (**D**) The gelatin hydrogel maintained its structural integrity, enduring more than 70% of compressive strain without breaking. (**E**) The stress-strain curves resulting from cyclic compression tests were evaluated for the hydrogel (peak strain, 70%; loading speed, 1 mm/s) within the strain range of 60–70%. (**F**) Moldability and injectability of the hydrogels. (**G**) Calcein/PI staining was conducted following the coculture of ADSCs with (using transwell cell culture plate) or without hydrogels (control group with PBS added) for 1 day and 3 days. (**H**, **I**) The activity of ADSC before and after hydrogel injection was detected by Calcein/PI staining and CCK8 assay. Scale bar: 20 μm(**A**), 4 mm (**F**), 100 μm (**G**)

RG1.The liposomes' morphology and structure were revealed by the images obtained from transmission electron microscopy (TEM) (Fig. 2A). We observed that the liposomes exhibited spherical or elliptical shapes with uniform distribution at the nanoscale. The Zeta potential measurement of -28.3 mV indicated a slight stable negative charge of the liposomes (Fig. 2B). Particle size distribution analysis showed an average size of 146.1 nm for the liposomes, with a narrow size distribution (Fig. 2C). To determine the encapsulation efficiency of liposomes encapsulating SDF-1α and ginsenoside RG1 (lipoSDF&RG1), we used HPLC methods to measure the drug concentrations in lipoSDF&RG1 after dialysis and compared them with the initial added amounts. The encapsulation efficiencies of SDF-1α and RG1 in the liposomes were determined to be 86.4% and 95.2%, respectively. Dynamic light scattering measurements were conducted to determine the particle size distribution and polydispersity index (PDI) of the liposomes, which followed a normal distribution pattern with a PDI close to

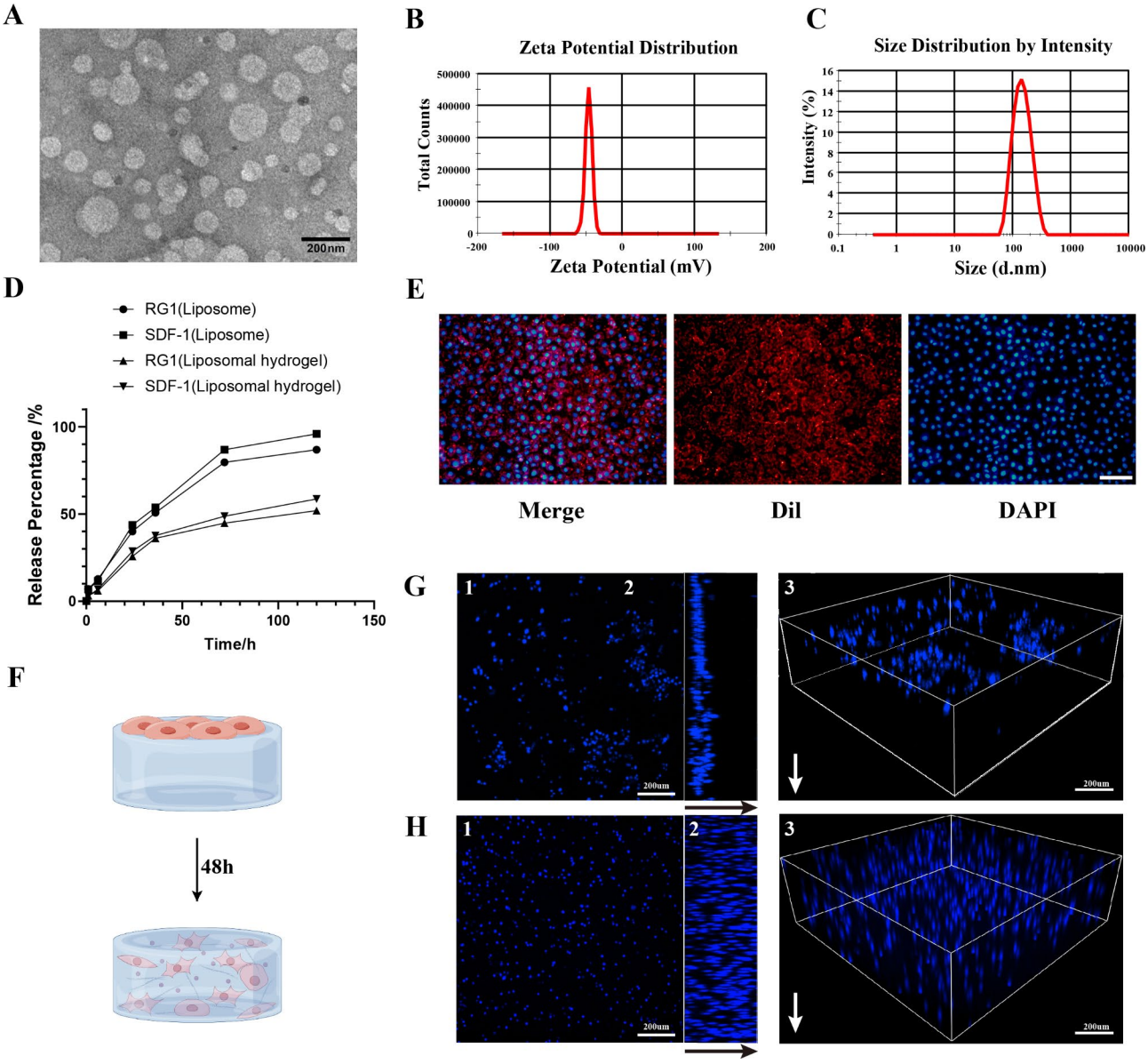

Fig. 2 Characterization of lipoSDF&RG1somes. (**A**) The cryogenic transmission electron microscopy (Cryo-TEM) analysis reveals predominantly globular, single-layered particles with an average diameter of approximately 100 nm in LipoSDF&RG1. (**B**, **C**) Size and zeta potential distributions of liposomes. (**D**) Release behavior of LipoSDF&RG1 and Gel@LipoSDF&RG1 loaded with SDF-1 and RG1 at 37 °C. (**E**) Fluorescent microscopy images demonstrate the absorption of liposomes by ADSCs following a 6-hour incubation period. Dil (red) was used to label the liposome membrane, while Hoechst 33,342 (blue) was employed to stain the cell nuclei. (**F**) Schematic diagram of three-dimensional cell culture in hydrogel. (**G**) Panel A1 presents a top view of the hydrogels consisting solely of ADSC. Panel A2 presents a representative image of the ADSC's position in the hydrogels (from top to bottom), and panel A3 represents the 3D image of the same. (**H**) Panel B1 displays a top view of the hydrogels containing ADSC and LipoSDF&RG1. Panel B2 exhibits a representative picture of the ADSC's location in the hydrogels (going from top to bottom), and panel B3 represents the 3D image of the same.Scale bar: 200 nm(**A**), 100 μm (**E**). 200 μm (**G**, **H**)

1, indicating a relatively uniform size of liposomes. The release kinetics of the liposomes at different time points were revealed by release curve experiments, demonstrating a gradually releasing and sustained characteristic (Fig. 2D). Incorporation of liposomes into hydrogels resulted in smoother drug release profiles and extended release durations, thereby prolonging drug efficacy and delaying their half-life. Fluorescent probe staining results showed that ADSCs successfully internalized the liposomes loaded with lipoSDF&RG1 after 6 h of co-culture (Fig. 2E). SDF-1 is an important chemotactic factor that induces directional migration of various stem cells. The gelatin hydrogel we have developed relies on host-guest complexation, which leads to the formation of flexible and fragile crosslinks that have the capability to enable cell migration and infiltration. ADSCs were seeded

on the surface of the hydrogel with or without loaded LipoSDF&RG1. After 48 h of incubation, most ADSCs without loaded LipoSDF&RG1 exhibited lower infiltration depth and slow proliferation (Fig. 2F, G), while most ADSCs in the group with loaded LipoSDF&RG1 infiltrated and migrated into the hydrogel, showing significant proliferation (Fig. 2G, H). Thus, we speculate that the gelatin hydrogel loaded with LipoSDF&RG1 can promote ADSC recruitment and migration, accelerating wound repair and regeneration.

The composite hydrogel supports the differentiation of ADSCs into nerves and inhibits the inflammatory polarization of macrophages

The abnormal immune microenvironment in the local area of diabetic wounds is an important factor contributing to their impaired healing, with the imbalance of M1/M2 macrophage ratio being a crucial aspect [23]. Therefore, we investigated the influence of LipoSDF&RG1 on macrophage polarization. After 24 h of M1 polarization induction in RAW264.7 (cultured in the presence of LPS (100 ng mL−1) and IFN-γ (20 ng mL−1)), they were subsequently treated with PBS, Gel, or LipoSDF&RG1 for another 24 h. Flow cytometry and immunofluorescence staining results indicated that the hydrogel loaded with LipoSDF&RG1 and ADSCs increased the proportion of M2 macrophages, while the group without loaded LipoSDF&RG1 did not show a significant increase in M2 polarization (Fig. 3A, H, E, F, G). Studies have already indicated the potent anti-inflammatory function of Rg1, which can synergistically regulate the balance between M1 and M2 macrophages [15, 24]. These findings reveal that LipoSDF&RG1 exerts its robust anti-inflammatory capacity by releasing Rg1. It can inhibit the polarization of M1 macrophages and promote their conversion to M2 polarization, thereby improving the inflammatory environment and facilitating wound healing.

We further investigated the effects of composite hydrogel loaded with ADSCs. In vitro studies were conducted to assess the impact of LipoSDF&RG1 treatment on ADSCs' neurodifferentiation. Nestin and β3-tubulin are classical marker proteins for neuronal cells. In the ADSCs from the PBS or hydrogel treatment groups, Nestin and β3-tubulin expression was barely detectable, indicating that ADSCs were unable to differentiate into neural progenitor/stem cells in the absence of neurodifferentiation signals (Fig. 3B, D). Conversely, within 7 days after LipoSDF&RG1 treatment, Nestin and β3-tubulin expression was detected in ADSCs, suggesting that Rg1 can induce stem cell differentiation into neuron-like cells. Furthermore, the qRT-PCR results validated this hypothesis. After culturing ADSCs in liposome-loaded gelatin hydrogels for three days, qRT-PCR results revealed higher mRNA expression levels of neurogenic markers Nestin, β3-tubulin, and Vimentin in the liposome-loaded hydrogel group compared to the control group and the hydrogel-only group (Fig. 3I, J, K). Previous studies have shown that ginsenoside Rg1 promotes ADSCs' neuronal differentiation [25, 26]. Through qRT-PCR results and immunofluorescence analysis of ADSCs' neurodifferentiation, we observed that the release of RG1 facilitated the differentiation of adipose-derived stem cells into mature neurons, which has a positive effect on wound healing.

The gelatin hydrogel promotes migration and angiogenesis of vascular endothelial cells

Angiogenesis and neovascularization are important links in wound healing. However, metabolic abnormalities caused by diabetes can lead to microvascular damage that delays healing [4]. Hence, we assessed the angiogenic characteristics of the complete regeneration system in vitro. The Human umbilical vein endothelial cells (HUVECs) were categorized into four groups: PBS (Control), hydrogel (Gel), hydrogel loaded liposome (Gel@LipoSDF&RG1), and hydrogel loaded liposome and ADSCs (Gel@LipoSDF&RG1/ADSCs). We co-cultured the composite hydrogel with HUVECs, with the HUVECs in the lower layer and the LipoSDF&RG1/ADSCs-loaded hydrogel containing the drug in the upper layer (Fig. 4A) (including tube formation, scratch test and Edu staining).

To test the ability of LipoSDF&RG1 to induce HUVEC migration, we first conducted Transwell migration and scratch tests. The results showed that both Gel@LipoSDF&RG1 and Gel@LipoSDF&RG1/ADSCs were able to induce HUVEC migration, with Gel@LipoSDF&RG1/ADSCs showing the most significant effect. However, no significant cell migration was observed in the PBS and Gel groups (Fig. 4B, C, D, G). As demonstrated by the Edu staining experiment shown in Fig. 4E H, the proliferation rate of HUVECs was higher in the Gel@LipoSDF&RG1 and Gel@LipoSDF&RG1/ADSCs treatment groups compared to the other two groups. Similarly, the angiogenesis assay showed enhanced blood vessel formation in the Gel@LipoSDF&RG1 and Gel@LipoSDF&RG1/ADSCs treatment groups (Fig. 4F, I), with Gel@LipoSDF&RG1/ADSCs showing the most pronounced enhancement effect. All these data indicate the synergistic potential of neural cells differentiated from ADSCs and the nanoliposomes LipoSDF&RG1 released by the hydrogel system in promoting cell migration and angiogenesis.

By simultaneously delivering ADSC and nano-drug liposomes, the gelatin hydrogel improved the healing of wounds in mice with diabetes

To further assess the effectiveness of hydrogel, we created a mouse model of long-term diabetic wounds to examine if the hydrogel system could expedite the healing process

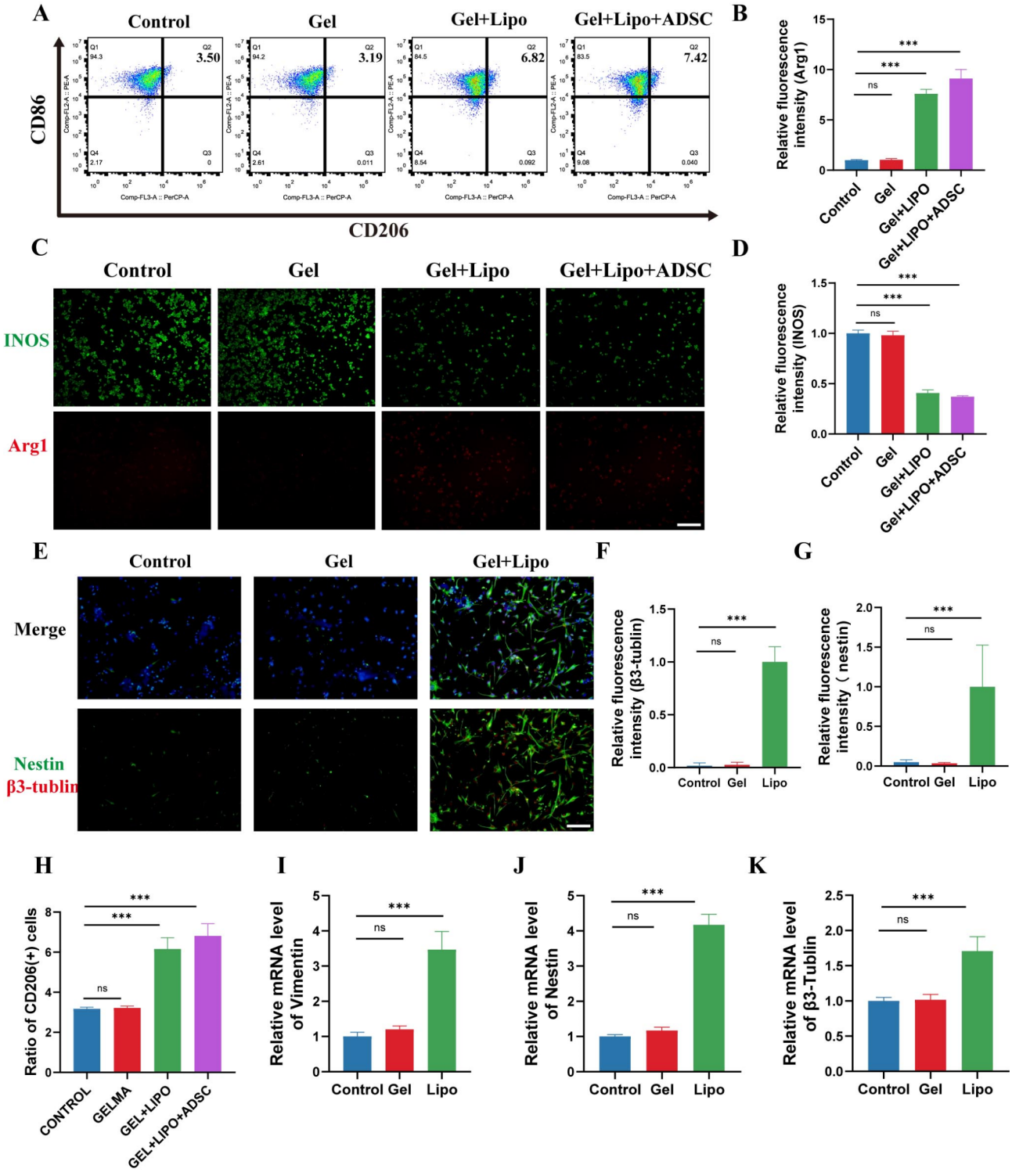

Fig. 3 The composite hydrogel supports the differentiation of ADSCs into nerves and inhibits the inflammatory polarization of macrophages. (**A**, **H**) After culturing RAW.264 cells in the presence of LPS and IFN-γ for 24 h, different treatment groups were further incubated for an additional 24 h. The proportion of M2 macrophages was measured by flow cytometry analysis (FCM). (**B**, **C**, **D**) The immunofluorescence images and statistical results of iNOS (M1, green) and Arg1 (M2, red) after processing RAW.264 cells as described in figure A. (**E**, **F**, **G**) After culturing ADSCs for 7 days in gelatin gels with different components, the neurogenic enhancement effect of LipoSDF&RG1 was detected by immunofluorescence staining of nestin and β3-tubulin. (**I**, **J**, **K**) After culturing ADSCs for 3 days in gelatin hydrogels with different components, the mRNA expression levels of neurogenic markers, namely nestin, β3-tubulin, and Vimentin, in different treatment groups were examined. Scale bar: 100 μm (**C**), 50 μm (**E**)

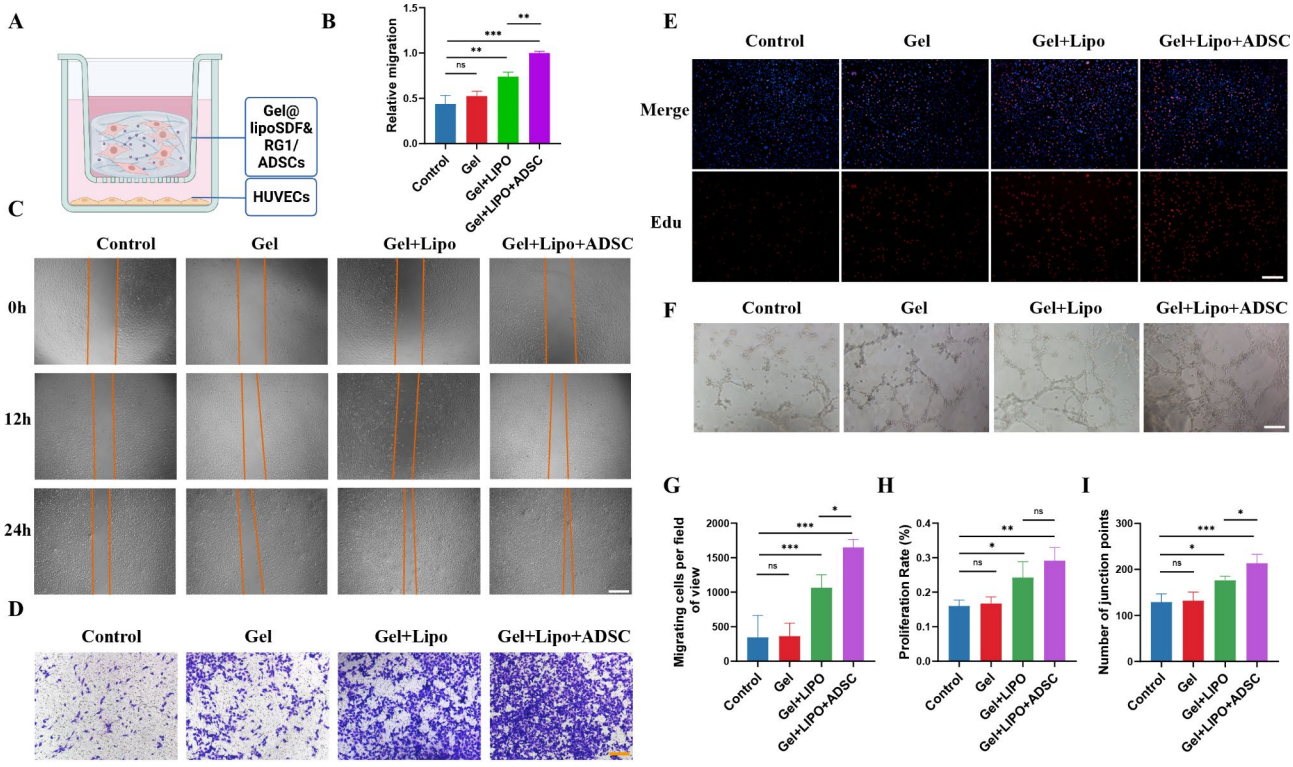

Fig. 4 Co-culture of composite hydrogel with HUVEC (tube formation, scratch, transwell, WB, etc.). (**A**) The diagrammatic representation of the co-culture setup. (**B**, **C**) The scratch wound closure assay was employed to evaluate the migratory capacity of HUVECs following specific treatments. (**D**, **G**) The migration ability of HUVECs in different groups was also detected by transwell assay. (**E**, **H**) Edu staining was used to assess the growth of HUVECs in various categories. (**F**, **I**) The angiogenesis ability of HUVECs in different groups was detected by tube formation assay. Scale bar: 200 μm (**C**), 100 μm (**D**, **E**, **F**)

in diabetic mice. A histological analysis was conducted to assess the development of fresh epithelium and granulation tissue. Figure 5 A shows that Gel@lipoSDF&RG1 and Gel@lipoSDF&RG1/ADSCs groups had significantly thicker granulation tissue than the control group. Different levels of collagen deposition were observed at the wound healing site through Masson's trichrome staining, with the Gel@lipoSDF&RG1/ADSCs group exhibiting the most significant deposition (Fig. 5B). Photographs of the injuries were taken on day 0, 3, 7, and 14 following the simulation (Fig. 5C, D). The statistical analysis indicated that the groups Gel@lipoSDF&RG1 and Gel@lipoSDF&RG1/ADSCs exhibited a considerably greater wound closure rate compared to the remaining groups.

Moreover, the collected wound tissue from various groups underwent immunohistochemical (IHC) staining for CD31. The histological examination of the stained tissues showed that there was an increased amount of blood vessels positive for CD31 in the regenerative region of the group treated withGel@LipoSDF&RG1 and Gel@LipoSDF&RG1/ADSCs, in comparison to the group that did not receive treatment (Fig. 5E, F).

In addition, we assessed the expression of neural cell markers (nestin and β3-tublin) in wound tissues using immunofluorescent staining. The findings indicated a notable increase in neural peptides in the Gel@lipoSDF&RG1 and Gel@lipoSDF&RG1/ADSCs groups (Fig. 6D, E, F). Gel@lipoSDF&RG1 effectively recruited ADSCs to the wound and enhanced peripheral nerve regeneration around the wound. Furthermore, the assessment of M1 or M2 macrophage activation phenotype involved the examination of the levels of inducible nitric oxide synthase (iNOS) (an indicator of M1) and arginase 1 (Arg1) (an indicator of M2). Immunofluorescence staining results from skin sections indicated a marked reduction in iNOS expression and a significant increase in ARG1 fluorescence intensity in the Gel@lipoSDF&RG1 and Gel@lipoSDF&RG1/ADSCs groups compared to the control group, suggesting a noticeable transition of macrophages towards the M2 reparative phenotype (Fig. 6A, B, C). The expression of IL-6 and TNF-α in the wound tissue was evaluated by Western Blot (WB). The results indicated that the levels of these two inflammatory factors were significantly higher in the control group and the gel group than in the Gel@lipoSDF&RG1 group and the Gel@lipoSDF&RG1/ADSCs group (Figure S2). In conclusion, these findings in the diabetic wounds (DWs) mouse model suggest a potent pro-healing effect of Gel@lipoSDF&RG1/ADSCs on diabetic wounds. After different treatments for 14

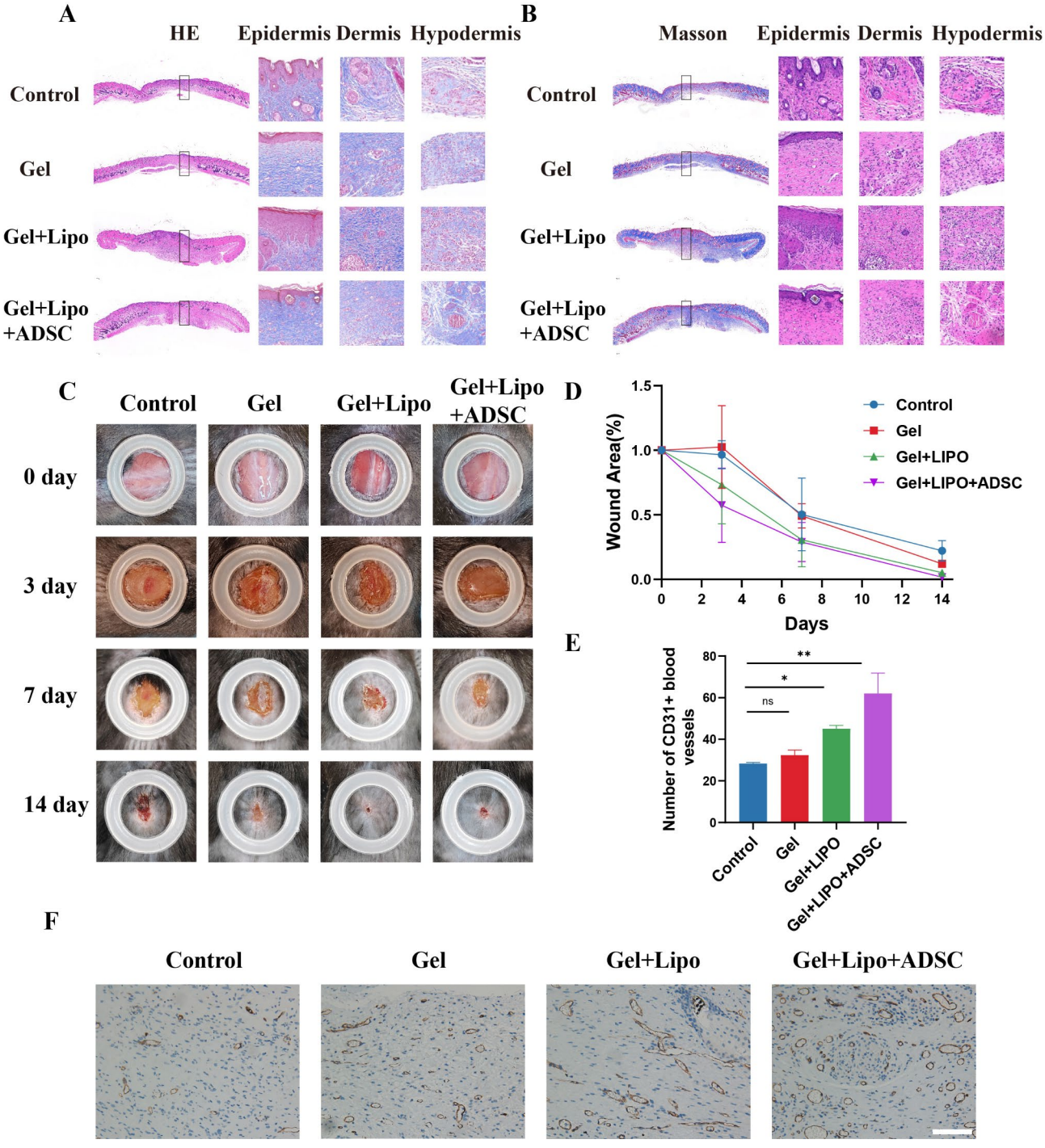

Fig. 5 Effect of the hydrogel system on diabetic mouse model. (**A**) H&E and (**B**) Masson's trichrome staining evaluation of wound regeneration following different treatments on the 14th day of post-wounding. (**C**, **D**) Representative pictures of complete-thickness wounds in diabetic mice at 0, 3, 7, 10, and 14 days after receiving treatment with Control, Gel, Gel@ lipoSDF&RG1, and Gel@ lipoSDF&RG1/ADSCs. (**E**, **F**) Immunohistochemical images showing CD31 expression in wound tissue. Scale bar: 200 μm (**F**)

days, the major organs of mice were stained with H&E. The results showed that the treated groups did not show any notable tissue damage in comparison to the control group, suggesting the exceptional biocompatibility of this hydrogel system (Figure S3).

Discussion

Biopolymer hydrogels have gained widespread usage as carriers for therapeutic cells and drugs in the field of biomedicine. Gelatin, in particular, is extensively employed due to its biocompatibility, bioactivity, biodegradability,

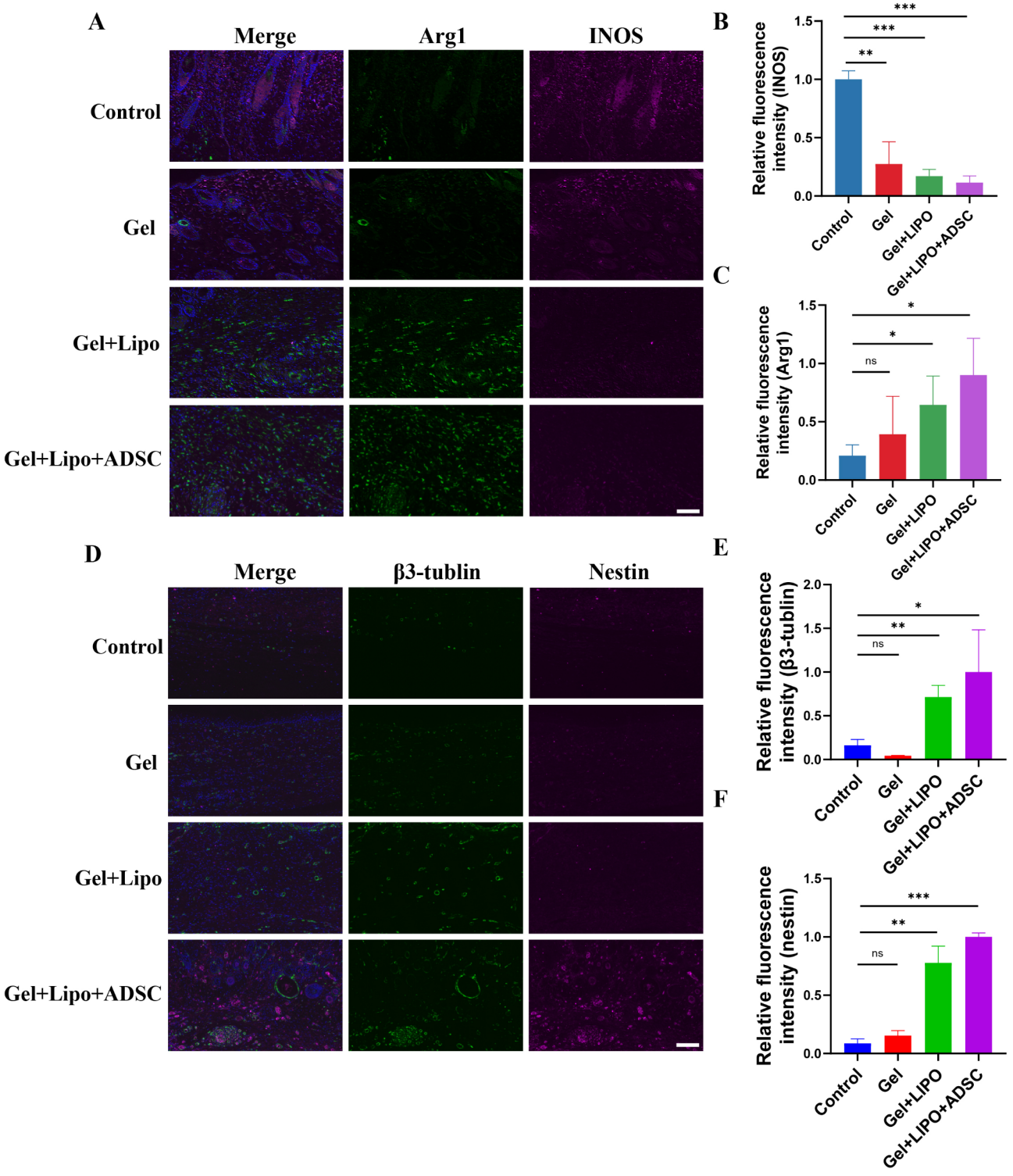

Fig. 6 Nerve repair and M2 polarization of macrophages in diabetic mice induced by gelatin hydrogel. (**A**, **B**, **C**) At day 14 after the wound, the skin tissues were examined using immunofluorescence imaging and the statistical data for Arg1 and INOS. (**D**, **E**, **F**) At day 14 after the wound, the skin tissues were examined using immunofluorescence images and statistical analysis to determine the presence of β3-tublin and Nestin. Scale bar: 100 μm (**A**, **D**)

and availability [27, 28]. However, traditional chemically cross-linked gelatin hydrogels exhibit poor mechanical properties and are not injectable [29]. To address these limitations, we have synthesized a highly dynamic host-guest complex as a physical cross-linking agent, enabling the development of injectable gelatin hydrogels with limited chemical cross-linking.

The hydrogel described achieves physical crosslinking primarily through weak yet highly dynamic host-guest interactions, complemented by limited chemical crosslinking to bolster stability. Specifically, synthesized photocrosslinkable acryloyl-β-cyclodextrin (Ac-β-CDs), capable of free diffusion, is linked to gelatin's aromatic residues (e.g., phenylalanine, tyrosine, and tryptophan) via host-guest interactions. Subsequent near-UV light-induced polymerization forms the gelatin hydrogel, where physical host-guest interactions between gelatin's aromatic groups and oligomeric Ac-β-CDs are distributed throughout the hydrogel network. Additionally, chemical crosslinking occurs sparsely and locally due to some Ac-β-CDs bearing multiple acryloyl groups.

The hydrogel exhibits shear-thinning behavior under stress conditions, transitioning to a "sol" state at high shear strains (e.g., approximately 1000%) and reverting to a "gel" state at subsequent low strains (e.g., 1%). This characteristic enables shear-thinning performance, facilitating smooth injection during administration. Upon extrusion from a needle, the hydrogel promptly recovers its "gel" state.

Further experiments have substantiated the exceptional dynamic properties exhibited by this gelatin hydrogel, which can be attributed not only to its physical host-guest crosslinking, encompassing remarkable attributes such as the ability to self-repair, superior compressive and tensile performance, injectability, and cell infiltration capacity, but also to its localized chemical crosslinking, thereby demonstrating ample stability for supporting the sustained three-dimensional cultivation of encapsulated cells.

Nerves and blood vessels play a critical role in the process of wound healing, and there exists a closely intertwined relationship between the nervous and vascular systems [2, 3]. The metabolic disturbances resulting from diabetes can lead to dysfunction in microvasculature and diabetic neuropathy, which are significant contributors to impaired wound healing in individuals with diabetes [4]. Moreover, the healing of wounds is characterized by a transition in the ratio of M1 to M2 macrophage phenotypes, signifying a shift from an inflammatory to a proliferative phase. In the context of diabetes, there is an elevated proportion of M1 (pro-inflammatory) macrophages to M2 (anti-inflammatory) macrophages, subsequently impeding the proliferative phase of wound healing [30].

Many published studies emphasize the importance of developing effective treatments for diabetic wounds. However, research on utilizing multifunctional hydrogels to regulate the neurovascular axis for promoting diabetic wound healing remains relatively scarce [6]. A recent study demonstrated how similar physical crosslinking methods enhance the stability and functionality of hydrogels, consistent with our hydrogel system [31]. Furthermore, other studies have highlighted the crucial role of SDF-1α in promoting cell migration and proliferation [32, 33], akin to the efficacy shown by SDF-1α loaded in our hydrogel carrier. Additionally, ginsenoside Rg1 has been validated in other studies for its ability to promote neuronal differentiation of ADSCs and regulate the high inflammatory immune microenvironment of diabetic wounds [12, 34].

Therefore, we developed a hydrogel composite therapy delivery system that incorporates adipose-derived stem cells (ADSCs) and nanoliposomes loaded with ginsenoside Rg1 and SDF-1α. The hydrogel provides an ideal environment for the growth, migration, and differentiation of cells, while SDF-1α promotes cell migration and proliferation, and Rg1 facilitates the neural differentiation of ADSCs while regulating the high inflammatory immune microenvironment of diabetic wounds. Initially, we assessed the biocompatibility of the hydrogel system and the 3D culture ability of ADSCs in vitro. Furthermore, we confirmed that the nanoliposomes promoted the neural differentiation of ADSCs and inhibited M1 polarization of macrophages, thus facilitating vascular migration. Subsequently, we further validated the therapeutic efficacy of this system on diabetic wounds using a mouse model. The results demonstrated that the system effectively activated ADSC migration and neural differentiation, improved the immune microenvironment of the wounds, and promoted vascular generation. In summary, our research provides a novel approach for the treatment of diabetic wounds. The unique crosslinking method of the hydrogel system not only offers a favorable environment for drug delivery, cell proliferation, and differentiation, but also possesses excellent mechanical properties and injectability, thereby providing a more convenient and effective strategy for clinical treatment of diabetic wounds.

Conclusion

In conclusion, the presented hydrogel-based therapeutic system represents a novel and integrated perspective for the management of diabetic wounds. By concurrently targeting immune response, angiogenesis, and nerve regeneration, this approach addresses the multifaceted challenges inherent in diabetic wound healing. The success of this innovative strategy opens avenues for further exploration, emphasizing the need for clinical translation

and continued investigation into the long-term efficacy and safety of the proposed cocktail therapy. Materials and methods.

Materials and methods

Synthesis of acrylate β-cyclodextrin (Ac-β-CD)

100 mL of DMF was used to dissolve 7 g of β-CD, followed by the addition of 5 mL of TEA to the solution. After stirring and cooling the resulting blend to a temperature of 0 °C, an additional 5 mL of acrylic acid was introduced. After being stirred for 10 h, the solution was filtered to eliminate trimethylamine hydrochloride. The clear solution obtained was subsequently concentrated to a volume of around 20 mL using a vacuum rotary evaporator. Then, the solution was gradually added to 600 mL of acetone, resulting in the precipitation of the altered β-CD. Subsequently, the solid was washed multiple times with acetone and subjected to vacuum drying for a duration of 72 h.

Preparation of hydrogel

Phosphate Buffered Saline (PBS) was used to dissolve Gelatin and Ac-β-CD, resulting in solutions containing 8% (w/v) gelatin and 10% (w/v) Ac-β-CD at a temperature of 37 °C. Afterwards, the compound I2959 was introduced at a 0.05% (w/v) concentration. Then, the resultant blend was transferred into Polyvinyl Chloride (PVC) molds at a temperature of 37 °C, and subsequently cooled down to 25 °C.To promote the development of supramolecular hydrogels, the mixture was subjected to ultraviolet (UV) light with a wavelength of 390 nm at an intensity of 5 mW/cm2 for a duration of 3 min at a temperature of 25 °C.

Rheological characterization

Rheological measurements were conducted using an Anton Paar MCR301 rheometer equipped with 25 mm diameter plates. The hydrogels were evenly spread between the plates with a 0.2 mm gap size. Gel behavior was observed over time through time sweeps performed at a strain level of 0.1% and a frequency of 10 Hz. The sample underwent sequential shear with a strain of 0.1% for 120 seconds, followed by 1000% strain for 60 seconds, for a total of 4 cycles, to conduct shear thinning tests. By performing time sweeps at a fixed frequency of 10 Hz, recovery of storage (G') and loss modulus (G") were monitored.

Tensile and compression mechanical analysis

The MACH-1 Micromechanical System was used to perform tensile tests on samples measuring 5 mm in width, 2 mm in thickness, and 10 mm in length. The specimens were firmly fastened, and the measure of tensile force was recorded while applying an extension rate of 1 mm/s. The samples were subjected to tensile fatigue tests, where they were exposed to a tensile strain of 60% at 25 °C or 100% at 37 °C for 10 cycles. Each cycle lasted for 30 s, and the tests were conducted at the same load speed. The MACH-1 Micromechanical System was used to conduct compression tests on samples measuring 3 cm in diameter and 3 mm in thickness. To measure the compressive characteristics, the specimens were compressed at a rate of 1 mm/s.

Hydrogel swelling/degradation test

The prepared hydrogels (200 μl) were immersed in 1 mL PBS at 37 °C. Subsequently, at specific time intervals of 1/2/6/12/24 hours, the surface water was removed, and the swelling samples were weighed. The swelling ratio was computed using the formula: swelling ratio = (Wt−Wd) / Wd × 100%, where Wd signified the dry weight of the hydrogel, and Wt represented the swollen weight. In addition, the degradation of the hydrogel was evaluated at specific time points of day 2, 5, 7, 19, and 14. After eliminating the surface supernatant, the weight of the hydrogel was measured, and the degradation ratio was calculated by the formula: degradation ratio=W1/W0×100%, where W0 indicated the initial wet weight of the hydrogel, and W1 represented the wet weight at a given time point.

LipoSDF&RG1some synthesis and drug loading

To form anionic lipoSDF&RG1somes, chloroform (Sigma, 10 mg/mL) was used to dissolve cholesterol, which was then combined with DSPC and DSPG at a molar ratio of 2:7:1, with both compounds at a 10 mg/mL concentration. The solution was left on a rotary evaporator overnight at 60 °C while slowly decreasing the pressure to 70 mbar using a nitrogen stream in order to eliminate the chloroform. Afterwards, the resulting slender lipid layer was rehydrated using a 1 mL solution of SDF-1α(12.5 μg/mL, Peprotech) and RG1(1 mg/mL, MCE) in PBS. To create lipoSDF&RG1somes of consistent size, the solution was vigorously mixed to create an emulsion and then passed through 200 nm polycarbonate membranes (Avanti, Canada) a total of 11 times.

LipoSDF&RG1 characterization

The LipoSDF&RG1 and hydrogel were analyzed under a Tecnai G2 20 transmission electron microscope (FEI, USA) after being treated with 1% uranyl acetate for staining to observe their morphology. The LipoSDF&RG1's size distribution and zeta potential were measured using a Malvern Zetasizer (Nano ZS, Malvern, U.K.). Weighed a certain mass of LipoSDF&RG1 and hydrogel accurately and placed them inside a dialysis bag (5000Da). Every group was submerged in a flask filled with one liter of PBS mixture and vigorously agitated at a temperature

of 37 degrees Celsius (100 revolutions per minute). This dialysis bag was taken out of the beaker at specific time intervals (specifically 6, 12, 24, 48, 96 h, 7, 14, and 21 days). Then, ten millilitres of the release medium solution was accurately drawn. The above-release medium solution was evaporated to dryness, then 0.5mL absolute ethanol was added and fully dissolved, and the supernatant was taken after rapid centrifugation (10000 rpm, 30 min). Following the filtration process, high performance liquid chromatography was utilized to detect SDF-1α/RG1, and subsequently, the drug release rate was determined for each group. The calculation of EE% is done indirectly using the formula : $EE\% = (m1-m2) / m1\times100$.

The initial mass of SDF-1α/RG1 used for membrane rehydration is represented by m1, while the mass of unencapsulated SDF-1α/RG1 identified through liquid chromatography is denoted as m2.

Cell culture and in vitro culture of hydrogels loaded with liposomes and ADSCs

The macrophage RAW264.7 cell line, obtained from mouse macrophages, and the HUVEC cell line, obtained from human umbilical vein endothelial cells, were acquired from the Cell Bank of the Chinese Academy of Science in Shanghai, China. The two cell lines were grown in a full medium that included 10% fetal bovine serum (FBS, Gibco, United States). Cells were subjected to D-Glucose (MCE, China) at 35 mmol/l concentration to simulate hyperglycemic conditions, while the control group was treated with glucose at a level of 5.6 mmol/l. Stem cells derived from mouse adipose tissue (ADSCs) were obtained from fat tissues located near the skin surface. The belly fat from 8-week-old C57BL/6 mice was gathered and placed in clean Petri dishes containing phosphate-buffered saline (PBS, Gibco, USA). After being minced and washed in Hank's solution containing collagenase type II (Sigma-Aldrich, USA), the tissues underwent digestion at 37 °C for 40–90 min until they reached a uniform texture. The process of cell isolation involved the use of a 70 μm nylon mesh for centrifugation and filtration. Afterwards, the cells were treated with a solution containing erythrocyte lysis buffer. Then, they were filtered again through a 40 μm cell strainer and suspended in a complete medium made up of DMEM enriched with 10% fetal bovine serum (FBS, Gibco, United States), 100 μg/mL penicillin, and 100 μg/mL streptomycin. Cells were incubated in a humid environment at a temperature of 37 °C and 5% CO2, with regular medium changes occurring every 2–3 days. Passaging of cells occurred once they achieved a confluence level of 70–80%.

The lipoSDF&RG1 were incorporated into the hydrogel solution to achieve appropriate drug concentrations of SDF-1α (approximately 5 μg/mL) and RG1 (approximately 400 μg/mL) in the hydrogel, and this drug-loaded liposome hydrogel was designated as the Gel@lipoSDF&RG1 group. For the Gel@lipoSDF&RG1/ADSCs group, adherent ADSCs were first digested and centrifuged. ADSCs at a concentration of 10,000 per microliter were uniformly mixed into the gelatin hydrogel, irradiated with 390 nm ultraviolet light (5 mW/cm², 3 min), followed by the addition of cell culture medium and incubation in a cell incubator for culture and subsequent experiments.

Assessment of the cell viability

After isolation and culture of ADSCs cells to a certain number and state. The prepared gelatin hydrogel was co-cultured with ADSCs cells using a transwell cell culture plate. ADSCs cells without the addition of hydrogel for co-culture were set as the control group (PBS was added). On the 1st and 3rd days after the end of co-culture, Calcein/PI staining kits (Beyotime, China) were used to stain the two groups of cells respectively according to the instructions of the reagent manufacturer. Finally, the staining results were observed and recorded under a fluorescence microscope, and the survival and death of cells were analyzed.

Furthermore, to investigate whether the hydrogel loaded with ADSCs can maintain the viability of the encapsulated cells during the injection process, after the synthesis of the hydrogel, we injected it through a G20 needle into a cylindrical mold to reshape the hydrogel. The reshaped hydrogel was cultured in vitro for 1 day and compared with the non-injected hydrogel cultured in vitro for 1 day through Calcein/PI staining and CCK8 assay. The Calcein/PI staining method was the same as mentioned above. When using the CCK-8 kit (Beyotime, China) to evaluate cell viability, the samples were cultured in a medium containing 10% CCK-8 solution at 37 °C for 2 h. The absorbance of the samples at 450 nm was measured using a microplate reader from BioTek, USA.

Flow cytometry

LPS stimulation induced RAW 264.7 cells to assume the M1 phenotype for a duration of 24 h, followed by a subsequent treatment of PBS, Gel, Gel@LipoSDF&RG1, or Gel@LipoSDF&RG1/ADSCs for an additional 24-hour period. After undergoing treatment and culturing, RAW 264.7 cells were collected, rinsed, and suspended in flow tubes. Cells were blocked by incubating with blocking buffer (Beyotime, China) for 20 min. Then, they were incubated with anti-F4/80 antibody (1:150, BioLegend, USA) conjugated with PE, anti-CD86 antibody (1:150, BioLegend, USA) conjugated with allophycocyanin (APC), and anti-CD206 antibody (1:150, BioLegend, USA) conjugated with FITC for 30 min. The analysis was

performed using a BD flow cytometer and evaluated using FlowJo software.

Reverse transcription-PCR

According to the protocol provided by the reagent supplier, quantitative reverse transcription polymerase chain reaction (qRT-PCR) was employed to measure the mRNA expression levels. The primer sequences for each gene were as follows: Nestin (forward primer: 5′GCAG AGAAGACAGTGAGGCAGATG-3′; reverse primer: 5′-GGAGGCAGGAGACTTCAGGTAGAG-3′), Vimentin (forward primer: 5′-CTGCTGGAAGGCGAGGAGA G-3′; reverse primer: 5′-TCAACCGTCTTAATCAGGA GTGTTC-3′), and TUBB3 (forward primer: 5′-CAGCGA TGAGCACGGCATAGAC-3′; reverse primer: 5′-CCAG GTTCCAAGTCCACCAGAATG-3′).

Cell immunofluorescent staining

Mesenchymal stem cells were placed onto confocal culture dishes with a concentration of either 4×104 or 2×104 cells per dish. The cells underwent treatment with PBS, Gel, or Gel@LipoSDF&RG1 for a period of 7 days. Afterward, the cells were rinsed with PBS in a gentle manner, then fixed in 4% paraformaldehyde for a duration of 15 min. Subsequently, they were subjected to 15 min of permeabilization with 0.1% Triton X-100, followed by a 30-minute blocking step using 10% goat serum (Boster, China). Overnight, the samples were then incubated overnight at 4 °C with primary antibodies targeting Nestin (Abcam, England) and β3-tubulin (Cell Signaling, China). The primary antibodies were detected by incubating them with FITC-conjugated goat anti-mouse IgG H&L (Beyotime, China) and CY3-conjugated goat anti-rabbit IgG H&L (Boster, China) at 25 °C for 2 h. In the end, the cells were stained again with DAPI and captured using a confocal fluorescence microscope from Olympus in Japan. Similarly, raw 264.7 cells were treated by different groups and then subjected to immunofluorescent staining using iNOS and Arg1 antibodies (Abcam, England).

Wound healing assay

HUVECs were cultured and seeded in six-well plates until they reached 90% confluence. Next, a sterile micropipette tip with a volume of 200 μL was utilized to generate an accurate scratch that was perpendicular to the surface of the well plate. Afterwards, the cell culture medium was discarded, and the plates were washed with PBS (three times). A medium without serum was included, and photographs were regularly captured at specific time intervals for documentation purposes. The extent of wound closure was quantified using ImageJ software for accurate analysis and assessment.

Tube formation assay

To assess the formation of the functional capillary network, HUVECs were treated differently and subsequently seeded in Matrigel-coated 96-well plates. Following a 6-hour incubation at 37 °C, images of formation of capillary-like structures were captured using an inverted microscope. The number of capillaries formed was quantified using ImageJ software, providing quantitative data for analysis.

EdU incorporation assay

Cell proliferation was assessed using EdU, a thymidine nucleotide analog, which was introduced into the cells. Following a 2-hour incubation period with EdU, HUVECs were fixed with 4% paraformaldehyde. Visualization of EdU incorporation was accomplished using an incorporation assay from manufacturer.

Transwell assay

The Transwell assay was conducted using 24-well Transwell chambers. HUVECs, suspended in a serum-free medium, were introduced into the upper compartment, while the lower compartment was filled with a complete medium. Different groups received equal volumes of PBS, hydrogel, Gel@LipoSDF&RG1, or Gel@LipoSDF&RG1/ADSCs added to the lower chamber. After incubating for 24 h, cells on the upper surface of the filter were carefully wiped off with a cotton swab. The cells that migrated to the lower surface were then stained with a 0.5% crystal violet solution. These migrated cells were subsequently observed and analyzed using an optical microscope.

Establishment of diabetic mice wound model

Approval for animal experiments on diabetic mice wound model was granted by the IACUC of Tongji Medical College, Huazhong University of Science and Technology (NO. 4083). 6-week-old male C57BL/6J mice were made diabetic by feeding them a high-fat diet for 6 weeks and then injecting them with streptozotocin (STZ; 40 mg kg^{-1} day^{-1}) for 7 days intraperitoneally. The diagnosis of diabetes was confirmed based on consistently high fasting blood glucose levels above 15.9 mmol/L. The mice were sedated with sodium pentobarbital (50 mg/kg; Sigma Aldrich), and circular skin wounds with a diameter of around 1 cm were surgically made on their dorsal region. Following the surgery, multiple subcutaneous injections totaling 100μL of drug or PBS were administered around the wound sites. Photographs of the wound were captured on days 0, 3, 7, and 14,, and the wound closure progress was evaluated using ImageJ software from Media Cybernetics, USA.

Histological analysis

We collected wound tissue samples from mice on days 3, 7, and 14 and promptly fixed them in 4% paraformaldehyde. After dehydration, these samples were embedded in paraffin sections for subsequent Hematoxylin and Eosin (HE) staining and Masson's trichrome staining. Additionally, for partial wound tissue paraffin sections obtained on day 14 postoperatively, antigen retrieval was performed by incubating in citrate buffer for 15 min, followed by blocking with goat serum for 30 min. Subsequently, the sections were incubated overnight at 4 °C with anti-CD31 antibody (1:100, Abcam), followed by DAB and hematoxylin staining. Finally, CD31-positive cells were counted under the microscope to evaluate the angiogenesis of the wound. Additionally, immunofluorescence staining using antibodies against INOS, Arg1, Nestin, and β-3 tublin (1:200, Abcam) were performed to assess their expression levels.

Statistical analysis

All the quantitative data were presented as mean ± standard deviation (SD). The significance was determined using the two-tailed student T-test or one-way ANOVA, with $P<0.05$. Each experiment was repeated at least three times.

Western blot analysis

Wound tissue samples were collected from each mouse group on the 10th day. The tissues were lysed with a buffer containing 1% protease inhibitors (Servicebio, China). Proteins were separated using SDS-PAGE and then transferred to polyvinylidene difluoride membranes. The membranes were blocked with 5% non-fat milk and incubated overnight at 4 °C with specific antibodies against ACTB, IL-6, and TNF-α (1:1000, Wanleibio, China). Following this, the membranes were washed and incubated for one hour at 23 °C with a goat anti-rabbit IgG antibody conjugated with horseradish peroxidase (1:1000, Cell Signaling, USA). Chemiluminescence was detected using the Western Blotting Detection kit for ECL (Byotime, China) as per the manufacturer's instructions to visualize the proteins.

Supplementary Information

The online version contains supplementary material available at https://doi.org/10.1186/s12951-024-03038-7.

Supplementary Material 1

Acknowledgements

Scheme 1 and Figure 4A were created with BioRender.com. Figure 2 F was created by Figdraw.

Author contributions

R.Z., Y.X., Z.L. and X.C.: conceptualization, methodology, and writing—original draft. B.L., L.L., C.L., J.L. and L.O.: methodology, data collection and analysis. Y.S., G.D., F.C. and G.L. : supervision, writing—review and editing. All authors reviewed the manuscript.

Funding

This work was supported by the National Science Foundation of China (No. 82272491, No. 82072444) ;National Science Foundation of Shenzhen (No. JCYJ20220531094802005); China Postdoctoral Science Foundation (NO. 2023M731217).

Data availability

No datasets were generated or analysed during the current study.

Declarations

Ethics approval and consent to participate

Approval for animal experiments on diabetic mice wound model was granted by the IACUC of Tongji Medical College, Huazhong University of Science and Technology. The experiments followed the ethical care and handling guidelines for laboratory animals established by the National Institutes of Health (NIH).

Consent for publication

Not applicable.

Competing interests

The authors declare no competing interests.

Received: 30 March 2024 / Accepted: 25 November 2024
Published online: 03 December 2024

References

1. Armstrong DG, Tan TW, Boulton AJM, Bus SA. Diabetic Foot Ulcers: a review. JAMA. 2023;330(1):62–75.
2. Pradhan L, Nabzdyk C, Andersen ND, LoGerfo FW, Veves A. Inflammation and neuropeptides: the connection in diabetic wound healing. Expert Rev Mol Med. 2009;11:e2.
3. Ivanov E, Akhmetshina M, Erdiakov A, Gavrilova S. Sympathetic system in Wound Healing: Multistage Control in Normal and Diabetic skin. Int J Mol Sci. 2023;24(3).
4. Elafros MA, Andersen H, Bennett DL, Savelieff MG, Viswanathan V, Callaghan BC, et al. Towards prevention of diabetic peripheral neuropathy: clinical presentation, pathogenesis, and new treatments. Lancet Neurol. 2022;21(10):922–36.
5. Nowak NC, Menichella DM, Miller R, Paller AS. Cutaneous innervation in impaired diabetic wound healing. Transl Res. 2021;236:87–108.
6. Xiong Y, Lin Z, Bu P, Yu T, Endo Y, Zhou W, et al. A whole-course-repair system based on neurogenesis-angiogenesis crosstalk and macrophage reprogramming promotes Diabetic Wound Healing. Adv Mater. 2023;35(19):e2212300.
7. Qin Y, Ge G, Yang P, Wang L, Qiao Y, Pan G, et al. An update on adipose-derived stem cells for Regenerative Medicine: where Challenge meets opportunity. Adv Sci (Weinh). 2023;10(20):e2207334.
8. Rautiainen S, Laaksonen T, Koivuniemi R. Angiogenic effects and Crosstalk of adipose-derived mesenchymal Stem/Stromal cells and their extracellular vesicles with endothelial cells. Int J Mol Sci. 2021;22(19).
9. Yuan X, Yuan W, Ding L, Shi M, Luo L, Wan Y, et al. Cell-adaptable dynamic hydrogel reinforced with stem cells improves the functional repair of spinal cord injury by alleviating neuroinflammation. Biomaterials. 2021;279:121190.
10. Tian T, Ko CN, Luo W, Li D, Yang C. The anti-aging mechanism of ginsenosides with medicine and food homology. Food Funct. 2023.
11. Xu FT, Li HM, Yin QS, Cui SE, Liu DL, Nan H, et al. Effect of ginsenoside Rg1 on proliferation and neural phenotype differentiation of human adipose-derived stem cells in vitro. Can J Physiol Pharmacol. 2014;92(6):467–75.
12. Dong J, Zhu G, Wang TC, Shi FS. Ginsenoside Rg1 promotes neural differentiation of mouse adipose-derived stem cells via the miRNA-124 signaling pathway. J Zhejiang Univ Sci B. 2017;18(5):445–8.
13. He F, Yu C, Liu T, Jia H. Ginsenoside Rg1 as an Effective Regulator of mesenchymal stem cells. Front Pharmacol. 2019;10:1565.
14. Long J, Liu XK, Kang ZP, Wang MX, Zhao HM, Huang JQ, et al. Ginsenoside Rg1 ameliorated experimental colitis by regulating the balance of M1/

M2 macrophage polarization and the homeostasis of intestinal flora. Eur J Pharmacol. 2022;917:174742.
15. Liu JQ, Zhao M, Zhang Z, Cui LY, Zhou X, Zhang W, et al. Rg1 improves LPS-induced parkinsonian symptoms in mice via inhibition of NF-κB signaling and modulation of M1/M2 polarization. Acta Pharmacol Sin. 2020;41(4):523–34.
16. Chen H, Li G, Liu Y, Ji S, Li Y, Xiang J, et al. Pleiotropic roles of CXCR4 in Wound Repair and Regeneration. Front Immunol. 2021;12:668758.
17. Chatterjee M, Gawaz M. Platelet-derived CXCL12 (SDF-1α): basic mechanisms and clinical implications. J Thromb Haemost. 2013;11(11):1954–67.
18. Fandel TM, Albersen M, Lin G, Qiu X, Ning H, Banie L, et al. Recruitment of intracavernously injected adipose-derived stem cells to the major pelvic ganglion improves erectile function in a rat model of cavernous nerve injury. Eur Urol. 2012;61(1):201–10.
19. Chen L, Yu C, Xiong Y, Chen K, Liu P, Panayi AC, et al. Multifunctional hydrogel enhances bone regeneration through sustained release of stromal cell-derived Factor-1α and exosomes. Bioact Mater. 2023;25:460–71.
20. Yang JW, Zhang YF, Wan CY, Sun ZY, Nie S, Jian SJ, et al. Autophagy in SDF-1α-mediated DPSC migration and pulp regeneration. Biomaterials. 2015;44:11–23.
21. Segers VF, Tokunou T, Higgins LJ, MacGillivray C, Gannon J, Lee RT. Local delivery of protease-resistant stromal cell derived factor-1 for stem cell recruitment after myocardial infarction. Circulation. 2007;116(15):1683–92.
22. Chacko IA, Ghate VM, Dsouza L, Lewis SA. Lipid vesicles: a versatile drug delivery platform for dermal and transdermal applications. Colloids Surf B Biointerfaces. 2020;195:111262.
23. Xiong Y, Mi BB, Lin Z, Hu YQ, Yu L, Zha KK, et al. The role of the immune microenvironment in bone, cartilage, and soft tissue regeneration: from mechanism to therapeutic opportunity. Mil Med Res. 2022;9(1):65.
24. Alolga RN, Nuer-Allornuvor GF, Kuugbee ED, Yin X, Ma G. Ginsenoside Rg1 and the control of inflammation implications for the therapy of type 2 diabetes: a review of scientific findings and call for further research. Pharmacol Res. 2020;152:104630.
25. Yuan T, Tan M, Xu Y, Xiao Q, Wang H, Wu C, et al. All-in-one smart dressing for simultaneous angiogenesis and neural regeneration. J Nanobiotechnol. 2023;21(1):38.
26. Ma J, Liu J, Wang Q, Yu H, Chen Y, Xiang L. The beneficial effect of ginsenoside Rg1 on Schwann cells subjected to hydrogen peroxide induced oxidative injury. Int J Biol Sci. 2013;9(6):624–36.
27. Kurian AG, Singh RK, Patel KD, Lee JH, Kim HW. Multifunctional GelMA platforms with nanomaterials for advanced tissue therapeutics. Bioact Mater. 2022;8:267–95.
28. Lv B, Lu L, Hu L, Cheng P, Hu Y, Xie X, et al. Recent advances in GelMA hydrogel transplantation for musculoskeletal disorders and related disease treatment. Theranostics. 2023;13(6):2015–39.
29. Yue K, Trujillo-de Santiago G, Alvarez MM, Tamayol A, Annabi N, Khademhosseini A. Synthesis, properties, and biomedical applications of gelatin methacryloyl (GelMA) hydrogels. Biomaterials. 2015;73:254–71.
30. Sharifiaghdam M, Shaabani E, Faridi-Majidi R, De Smedt SC, Braeckmans K, Fraire JC. Macrophages as a therapeutic target to promote diabetic wound healing. Mol Ther. 2022;30(9):2891–908.
31. Xu J, Feng Q, Lin S, Yuan W, Li R, Li J, et al. Injectable stem cell-laden supramolecular hydrogels enhance in situ osteochondral regeneration via the sustained co-delivery of hydrophilic and hydrophobic chondrogenic molecules. Biomaterials. 2019;210:51–61.
32. Yu JR, Varrey P, Liang BJ, Huang HC, Fisher JP. Liposomal SDF-1 alpha delivery in Nanocomposite Hydrogels promotes macrophage phenotype changes and skin tissue regeneration. ACS Biomater Sci Eng. 2021;7(11):5230–41.
33. Yu JR, Janssen M, Liang BJ, Huang HC, Fisher JP. A liposome/gelatin methacrylate nanocomposite hydrogel system for delivery of stromal cell-derived factor-1α and stimulation of cell migration. Acta Biomater. 2020;108:67–76.
34. Zhen J, Bai J, Liu J, Men H, Yu H. Ginsenoside RG1-induced mesenchymal stem cells alleviate diabetic cardiomyopathy through secreting exosomal circNOTCH1 to promote macrophage M2 polarization. Phytother Res. 2024;38(4):1745–60.

Publisher's note